

Biplanar Cardiac Blood-Pool Tomography

Stuart G. Mirell, Harvey S. Hecht, James M. Hopkins, and W. H. Bland

Veterans Administration Wadsworth Medical Center and University of California at Los Angeles, Los Angeles, California

Dynamic transverse axial wall tomograms of the left ventricle (LV) are reconstructed by a new technique from anterior and LAO views acquired with a conventional scintillation camera imaging the distribution of in-vivo Tc-99m-labeled red blood cells. By confining reconstruction to the singular contiguous uniform concentration of activity in the LV, the requisite angular samplings for a given level of accuracy are substantially reduced in this restricted form of emission computed tomography (ECT).

Static phantom studies using a series of volumes having various cross-sectional dimensions demonstrate tomographic edge reconstruction with $\leq 12\%$ rms radial error. The dynamic cardiac ECT is demonstrated in a series of representative patient studies by reconstruction of wall tomograms in the end-diastolic and end-systolic phases of the 28-frame cardiac cycle. In contrast to the conventional dual multiframe projection views, the motion tomograms derived from the reconstructions clearly show the complete three-dimensional perspective of wall displacement.

J Nucl Med 22: 913-920, 1981

The rapid development of cardiovascular nuclear medicine in recent years has prompted renewed interest in emission computed tomography (ECT) techniques that utilize a scintillation camera as the detector. The increased availability of on-line computers has provided the necessary processing capability.

The generalized ECT problem presumes an arbitrary distribution and concentration of radiotracer in a given cross section. The reconstruction in such a generalized case necessitates many sampling angles. The interrelationship between reconstruction accuracy and requisite angular sampling frequency has been extensively examined in the context of ECT (1-6) and other imaging disciplines as well (7,8), including transmission computed tomography (TCT).

A diversity of angular sampling techniques has been devised in order to adapt the scintillation camera to ECT. Keyes et al. (10) and Budinger et al. (4) rotate the subject, whereas Jaszczak et al. (11) rotate the camera head. For systems having both subject and camera head stationary, the maximum divergence of the angular samplings is necessarily restricted. Such systems would include the use of coded apertures (12-14), the rotating slant-hole collimator (15), and, most recently, the seven-pinhole collimator (16).

This investigation differs from standard approaches to ECT in that edge tomograms are subsequently reconstructed from totally conventional acquisitions of the Tc-99m-labeled blood pool (17). It will be shown that a set of very special conditions are met in gated left-ventricular (LV) blood-pool imaging, such that only two views—an anterior (ANT) and a 45° left anterior oblique (LAO)—are required for the computation of transverse tomograms. These views are acquired with a standard-view scintillation camera and LEAP parallel-hole collimator together with an on-line computer.

Received July 15, 1980; revision accepted June 8, 1981.

For reprints contact: Dr. Stuart G. Mirell (691/115), Nuclear Medicine Service, VA Wadsworth Medical Center, Los Angeles, CA 90073.

Consequently, the tomograms are an adjunctive diagnostic by-product derived from the conventional acquisitions, and do not alter the routine clinical procedure.

Lewis et al. (18) examined the related problem of sizing myocardial infarction from anterior and lateral technetium-99m stannous pyrophosphate scintigrams by using the projective areas of the detected infarcts. These authors recognized, however, that the information contained in the point-by-point count levels could not be exploited because of the nonuniform tissue uptake. They also noted that a sizing estimate of this nature excluded the determination of actual infarct shape.

A more recent investigation by Asahara et al. (19) did, however, address the same problem studied in this paper: the tomographic reconstruction from two views of the LV equilibrium blood pool. The algorithm these authors used presumed a regular LV shape composed of oval-arc cross sections with dimensions determined from the projective LV areas in LAO and RAO camera views 90° apart. This algorithm also did not utilize count levels, even though activity in a labeled blood pool is uniform. The authors identified the inherent limitations of their algorithm by examining phantoms that differed substantially from the presumed regularized LV shape.

In contrast, we present an algorithm that fully utilizes the information content of the measured count levels from the LV. The algorithm proceeds through a series of mathematical processes that simultaneously apply two constraints upon the manipulated data. The first constraint demands that the inherent information content of the data for each view remain unaltered. The second constraint imposes self-consistency upon the relative information content of the two views. Through a successive implementation of the constraints, arbitrary volumetric cross sections are reproducibly derived.

Principles. The ANT and 45° LAO views generally provide the most divergent pair of angular samplings that still maintain relative isolation of the LV with respect to RV overlap of the inferior wall. As a consequence, with the radiotracer in an equilibrium blood-pool distribution of the LV, detected counts are essentially proportional to LV volume after background correction.

This premise is operant when the ejection fraction is computed in conventional gated blood-pool studies that treat the (background-corrected) LV counts as proportional to LV volume for each frame in the cardiac cycle. A measure of the validity of this premise is provided by the accuracy of the ejection fraction derived from such studies. Nevertheless, estimates of the factors influencing count-to-volume proportionality were made with regard to a series of phantom studies. These factors relate to self-attenuation within the LV itself and to the mean attenuation from overlying tissue. The latter introduced a common factor to all frames of a given view and so did not influence proportionality but did alter the ratio of counts detected from the two views, each of which gen-

erally incurred a different overlying attenuation. Accordingly, for each view and transverse level sampled, mean attenuation factors that correct for this overlying tissue are implicit in the reconstruction algorithm. The factor relating to self-attenuation was found to influence proportionality only minimally as a result of compensating aspects in the detection process. Estimates of the residual error introduced by self-attenuation are treated below with regard to results of the phantom study.

The proportionality relationship is also valid in relating a local observed count density in the LV to the corresponding physical dimension or geometrical chord of the LV cavity in the direction perpendicular to the plane of view. The observed count density is derived from the fractional LV blood pool contained within an imaginary volume cell of unit cross section and with a length equal to the chord.

A transverse linear array of these cells is sampled simultaneously by using a profile-analysis program on a single frame from a particular view. The detected count densities are displayed and stored in a curve format. The amplitudes along such a curve are then proportional to the corresponding chord lengths, as illustrated in Fig. 1.

For reconstruction, two count-profile curves are generated from an ANT and an LAO data frame, respectively, at identical temporal phases of the cardiac cycle. The vertical positioning of the sampled band for the two frames must also be identical. Taken together, such a pair of curves determines two complete coplanar sets of parallel transverse chords. On the LV cross section in Fig. 1, the ANT and LAO sets of chords are depicted by the long axes of the vertical and oblique cells, respectively. Given adequate angular divergence of views,

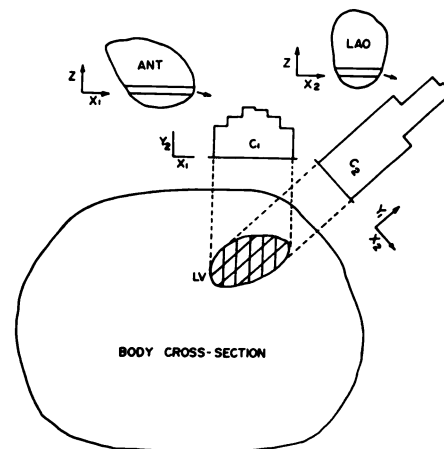


FIG. 1. Body cross section illustrating geometrical relationships of LV chord dimensions, profile curve amplitudes, and associated projection views for a single transverse level at a particular phase of the cardiac cycle. Note the proportionality of the LV vertical and oblique cell lengths (chords) to the amplitudes of C_1 and C_2 , respectively.

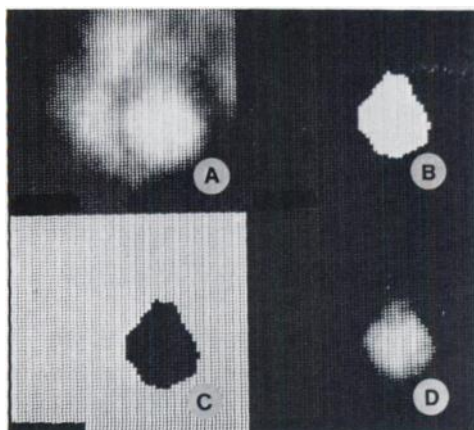


FIG. 2. Preprocessing sequence for single data frame (e.g., LAO ED). (A) Original data frame; (B) computer-generated LV area; (C) negative mask of LV area; (D) isolated LV with background correction.

these two sets then comprise the necessary and sufficient information for a tomographic reconstruction of a single transverse LV perimeter. Since maximal angular divergence is restricted by visualization of the septum to approximately 45° , the adequacy of this divergence will be examined by phantom studies with regard to reconstruction accuracy. The reconstruction entails computation of a single contour that simultaneously satisfies the chord dimensions of each set. Such a reconstruction is virtually confined to the singular, albeit significant, application of cardiac ventricular blood pool, because the activity must be uniformly dispersed in a contiguous isolatable distribution.

METHODS

The blood pool is labeled *in vivo* by the administration of 3 mg Sn^{2+} followed by the injection of 25 mCi sodium pertechnetate (Tc-99m). After equilibrium distribution, the heart is imaged with a scintillation camera* using a low-energy all-purpose parallel-hole collimator. Data from the central quadrant of the camera crystal are acquired by the computer[†] together with an R-wave logic pulse. The cardiac cycle is formatted into a 28-frame sequence averaging 150 K counts/frame on 64×64 matrices. The ANT and 45° LAO views are each acquired in approximately 6–10 min.

Specific aspects of this procedure, such as labeling technique and framing rate, may be altered without critically affecting the subsequent tomographic reconstruction. However, it is essential to acquire enough count density (on the order of several hundred cts/cm^2) in order to optimize reconstruction accuracy. In addition, the septum should be well visualized in the ANT and LAO views. These requirements do not generally impose any difficulty, since they are consistent with diagnos-

tically significant conventional projective LV gated studies.

Algorithm data preprocessing. Before tomograms can be reconstructed, the data frames in the ANT and LAO studies are first preprocessed using the standard analysis program for gated LV blood-pool studies provided in the computer[†] software. This program uses a combination of second derivative and threshold to define the LV edge for each data frame. All matrix points interior to this edge are then assigned by the program as the corresponding projective area of the LV. A single data frame and the derived area are shown in Figs. 2A and 2B, respectively. A background sampling over a band of matrix points immediately to the right of the defined area shown in Fig. 2B is then applied to the data frame of Fig. 2A. The average count per matrix point in this sampling is subtracted from the data frame.

Final preprocessing is carried out using additional standard software programs. A matrix "mask," Fig. 2C, exterior to the projective area, is generated and used to isolate the (background-corrected) LV. This final form of the preprocessed frame, shown in Fig. 2D, constitutes a portion of the necessary data input for tomographic reconstruction.

In a restricted two-phase reconstruction procedure, wall tomograms are computed only for the ED and ES frames of the cardiac cycle. Accordingly, the data preprocessing described above is applied to four data

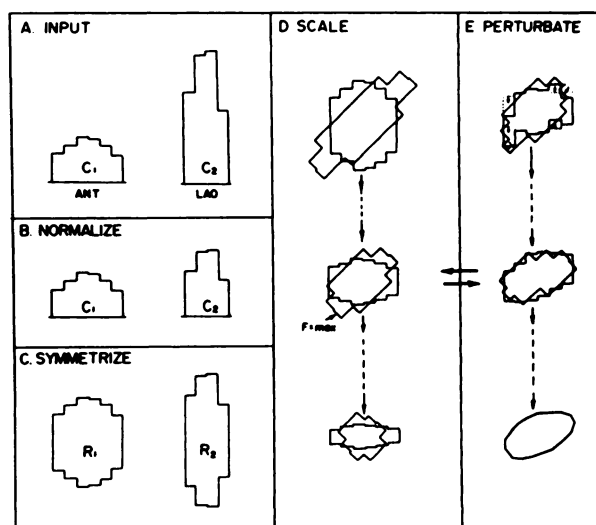


FIG. 3. Schematic of processing sequence for single tomogram. (A) Input profile curves from same level of corresponding preprocessed ANT and LAO data frames. (B) Normalize by imposing integral equivalence. (C) Generate mirror-symmetric contours by adding negative-valued curve amplitudes. (D) Superimpose contours oriented at corresponding acquisition angles and scale Y axes simultaneously to maximize ratio F of overlap region to all-inclusive region. (E) Remove mirror symmetry constraint by translational perturbation of individual contour amplitudes along the respective Y axes to maximize F further. Iterate to previous step until maximum convergence is achieved.

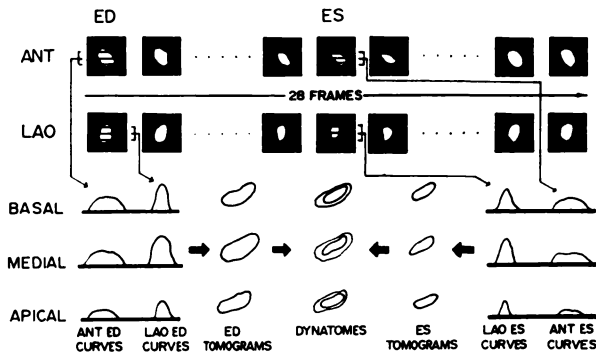


FIG. 4. Flow diagram showing overall relationship of original gated acquisition frames to the final set of dynatomes reconstructed for the end-diastolic and end-systolic phases of the cardiac cycle.

frames: ED and ES for ANT and LAO. A multiphase reconstruction applied to all data frames in both views would provide a time continuum of tomographic images for the entire cardiac cycle, but this is deferred at present because of an order-of-magnitude increase in processing time over that for the two-phase reconstruction. In addition, a hard-copy film presentation of tomographic wall excursion is most clearly demonstrated by the superposition of the corresponding ED and ES tomograms from a given level of the LV—a “dynatome.” Superposition of multiphase tomograms tends to obscure the perception of wall-segment transients, particularly when paradoxical motion is present.

Tomographic reconstruction. This proceeds pairwise from single-phase (ED or ES) ANT and LAO profile sampling curves derived from a given level such as C_1 , C_2 , in Fig. 1 and again in Fig. 3A.

Generally, three transverse profile curves are generated at regular longitudinal intervals from each of the four preprocessed data frames. The sampling region for each curve corresponds to a 1-cm-high horizontal band across the LV. Each tomographic study would then comprise 12 such curves, as shown in Fig. 4.

Because of the preprocessing routine, these curves are zero-valued beyond the LV border. The number of nonzero sample points on a given curve correlates with the transverse projective dimension of the LV at the level sampled. In general, the number of nonzero sample points for an ANT and LAO curve pair, n and m , respectively, will be different, with m typically somewhat larger than n for anatomical reasons.

Self-consistency demands that the total integral of counts for the curves in a pair be equal, since the same transverse volume slice is sampled by both profiles. Because of differences in the overlying tissue attenuation associated with the two projections, integral equality must be achieved by normalizing one of the curves in a pair to the other by a single multiplicative factor derived from the initial integral ratio (Fig. 3B).

A pair of mirror-symmetric contours is generated

from the pair of normalized curves by assigning a negative y value equal to each of the n (or m) sample points along the x axis (Fig. 3C). The vertical dimension of a contour (and, of course, the original curve) at each sample point is proportional to the associated chord length of the LV described earlier. In this respect, the contours are each a first approximation to the true wall tomogram. The constant of proportionality is determined by computing a single numerical multiplicative factor for the contour pair that scales the y dimensions with respect to the x dimensions. The number of sample points along the x axis already correlates with the physical width of the LV projection, since the linear interval per matrix point is easily determined from a bar-phantom image. Scaling has the effect of bringing the y dimension of each contour into proper physical proportion with the x dimension.

An initial value of the scale factor is computed from a superposition of a contour pair, Fig. 3D, with the LAO contour rotated by 45° corresponding to the difference of the associated acquisition angles of the scintillation camera. The contours will have areas with mutual overlap and with nonoverlap. It is the ultimate objective of this reconstruction to modify the contour pair so that convergence is achieved toward a single contour that constitutes a single wall tomogram. Convergence must be achieved in a manner consistent with the physical principles of the data acquisition. Specifically, in the case of scaling, overlying tissue attenuation is an unknown parameter, so the total counts may be scaled as a single degree of freedom to maximize a convergence. This operation is functionally equivalent to simultaneous compression or expansion of the respective y axes of the contours, as shown in Fig. 3D. Convergence in this subroutine is evaluated by the function

$$F = \frac{\int R_q dx dy}{\int R_Q dx dy}$$

The integrand functions R_q and R_Q refer, respectively, to the overlapping contour region and the all-inclusive region of both contours; the numerator and denominator are integrals that yield the respective areas of these regions. At some intermediate scale factor, the ratio of the area integrals in F approaches unity, indicating maximum convergence (as indicated in the middle diagram of Fig. 3D).

There are, additionally, $n + m$ degrees of freedom in maximizing the contour convergence, where n and m are, as before, the number of sample points, respectively, for the pair of contours. In the acquisition process, each sample point derives its counts from an oblong parallelepiped volume cell with the long dimension of the cell being the chord spanning the LV and perpendicular to the image plane. The mean “depth” of each cell is an undetermined parameter given data for only a single

view or projection. That is, the cells of activity for a given projection can be shifted parallel to each other with no significant alteration in the acquired data. Consequently, these chords may be perturbed independently by translations along the respective projection axes on the contour superposition to increase the relative contour overlap, as illustrated by the first two diagrams in Fig. 3E.

Functionally this operation is represented by the addition of a perturbation term P_N to the scaled contours, thereby redefining them in a nonsymmetrical form. The symmetry constraint is removed by the added P_N terms that correlate with the Y-axis translations at the corresponding X_N maximizing F. The data are then scaled and perturbed again, iteratively, to maximize F further.

All of the above computational processes do not at any time alter the original relative amplitudes of either profile curve. These original relative amplitudes can be retrieved at any stage of the processes from the amplitudes of the modified curves or from the contour dimensions measured along the corresponding axis of acquisition.

From the final, nearly convergent contours, a single mean-value contour (third diagram in Fig. 3E) is defined, which constitutes one tomogram. A total of six such tomograms typically comprises a full set for a given study consisting of three pairs of ED and ES tomograms derived from the lower, middle, and upper transverse segments of the LV (Fig. 4).

Because a full set with the present computer programs requires more than an hour of operator processing time, for practicality the iterations have been truncated at two or three cycles. However, most of this time is occupied with transference of data between a series of computer subroutines. With complete automation of all phases of the reconstruction, a complete study would require only several minutes of processing time.

RESULTS

The algorithm presented above yields a dynamic representation of LV wall tomograms. However, the process is inherently a static reconstruction from paired frames from divergent projections at identical temporal phases. The dynamic aspect is derived from repeated applications of the reconstruction process to two or more frames in the multiple-frame gated acquisitions.

Accordingly, static phantom studies offer one potential means for validating the reconstruction accuracy of the algorithm. The phantoms consist of a series of vessels having various cross sections.

The results reported here include two preliminary studies using a 150-ml spherical flask (6.6-cm diameter) and a 110-ml cylinder of elliptical cross section (4.9-cm major axis). These studies were followed by the some-

what more demanding reconstruction problem presented by an asymmetric phantom immersed in a scattering medium.

An activity of only a few μCi is required in order to generate images in several minutes with count densities comparable to those from the LV in patient studies. The ANT and 45° LAO views are simulated by acquisition of a static image followed by a 45° rotation of the phantoms about their vertical axes and acquisition of a second static image.

The profile samplings of the two preliminary phantom studies, necessarily orthogonal to the vertical axes of rotation, intersect circular and elliptical cross sections, respectively, on the phantoms. The unmodified profile curves qualitatively demonstrate certain basic aspects of the reconstruction algorithm.

The critical count-to-chord proportionality may be verified by demonstrating that an appropriate y-axis scale factor conforms either of the sphere's profile curves to a semicircle. Because of the geometrical simplicity of the sphere, this single operation of scaling essentially generates the tomogram.

The A and the A + 45 views of the cylinder are analogous to the ANT and the LAO views of the LV in the respect that the major axis of the grossly elliptical LV cross section is approximately parallel to the LAO line of projection. Accordingly, LV profiles are characteristically sharply peaked in LAO (looking "down" the major-axis chord) and somewhat broader in ANT (off-axis). The cylinder phantom simulates these characteristics, as evidenced by the bottom profile curves in Fig. 5A.

Accuracy of the final phantom tomograms is assessed by calculating the radial error. When the computer-reconstructed tomogram and the true cross section ob-

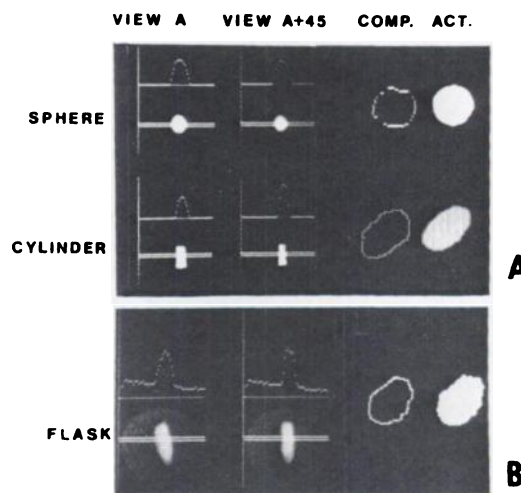


FIG. 5. Phantom studies of (A) sphere and elliptical cylinder and (B) asymmetric phantom. Shown are: profile pairs with associated projective images, computer reconstructed wall tomograms, and actual cross sections.

tained from an actual physical measurement of the phantom are superimposed at their respective geometric centers, the perimeters will not precisely overlap. The radial difference (gap) between these perimeters at a given angle, divided by the true radius at that angle, provides a single percent error sampling. Integrating the root-mean-square sum over 2π then provides a measure of the total average radial error. The percent standard deviations for the sphere and the cylinder are 9% and 11%. The corresponding spatial error is approximately 7 mm.

The final phantom study reported here used an irregularly deformed 190-ml polypropylene flask (5 cm maximum cross-sectional diameter) submerged in a 40-l water bath. Enough activity was added to the water bath to provide the typical target-to-background ratio associated with a conventional cardiac blood pool. The asymmetric cross section of the polypropylene flask, together with the presence of a radioactive (Tc-99m) scattering medium, provided a phantom study approximating that of the static LV.

The profile samplings of this study are shown in Fig. 5B. The central axis of the flask was inclined 30° from the vertical to further simulate LV imaging conditions.

An advanced version of the reconstruction algorithm was used to obtain the final tomogram shown in Fig. 5B. The essential improvement in this algorithm was the inclusion of a correction providing variable background sampling and interpolation. For each profile curve, background data points exterior to the phantom on the left and on the right were sampled. A background subtraction value for each intermediate data point on the profile curve was then computed by linear interpolation of the left and right sampling. By this process variable background across the entire field of view is compensated by the reconstruction algorithm. The final reconstruction of the irregular phantom was then compared with a physical measurement of the phantom contour taken at the corresponding oblique (30°) cross section. The rms radial error was approximately 12% for this study.

Error arises primarily from the finite resolution of the camera, and secondarily from self-attenuation within the LV pool. Estimates of the latter contribution to the error were made for the phantom studies at the 140-keV energy. Self-attenuation introduces an error as a result of deviation in count-to-volume proportionality. In a given view, the sample cells will differ substantially in length, diminishing to zero at the LV periphery and reaching a maximum in the central portions of the LV. The mean depth of these cells, however, will be relatively constant. The shorter peripheral cells will have negligible self-attenuation, whereas the longer cells will suffer a self-attenuation that is a function of the position along the cell length. This function is generally highly nonlinear, being proportional to the hyperbolic sine centered at the

mean cell depth. (This is a straightforward exercise in integrating the exponential attenuation function along the cell length.) Accordingly, because of nonlinearity one would not generally expect the less-attenuated activity in the upper portion of the cell to offset the more-attenuated activity in the lower portion of the cell. However, at the 140-keV energy and for cells approximating 7 cm or less in length (as in the phantoms and the typical LV), the hyperbolic sine is in a highly linear range, such that the variances in attenuation very nearly compensate and the resultant detected counts are within 2% of what they would have been without the effects of self-attenuation.

Following the initial phantom work, a preliminary series of 20 patient studies was selected from the computer data storage discs for tomographic evaluation. The ED and ES frames from the ANT and LAO conventional gated blood-pool views are routinely maintained on permanent storage. Consequently, tomograms can be generated at any time subsequent to acquisition. Several of these reconstructions are shown in Figs. 6 and 7. The format for a complete study consists of the four original data frames (ANT and LAO of ED and ES) and the dual computer-generated areas for each view. The four dynatomes on the right appear in progressive equispaced order from apex to base (as indicated by the apical distance). The reconstructions are derived by sampling bands 1 cm high in profile.

Owing to the uniqueness of the tomographic reconstructions, no direct validation is readily available. Subjective regional and wall-motion assessment from the available complementary angiographic studies and the original gated blood-pool images offer a measure of indirect corroboration. Furthermore, because of the

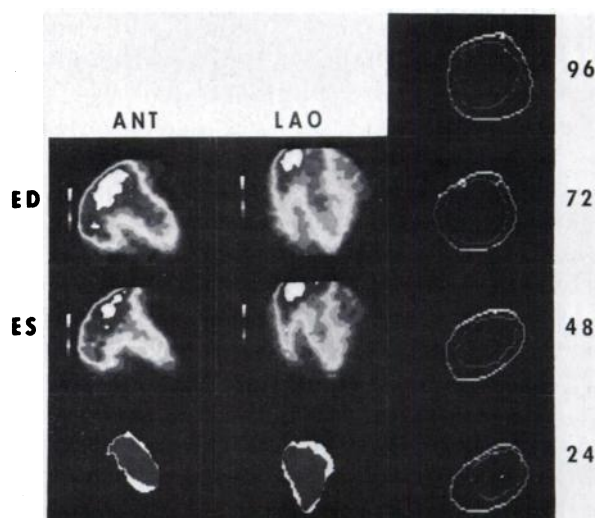


FIG. 6. Case study of anterior-wall hypokinesis. First two vertical columns show, respectively, ANT and LAO sets of ED and ES data frames and superimposed computer-generated areas. A series of four tomographic wall reconstructions referenced in mm to apex is shown in third column.

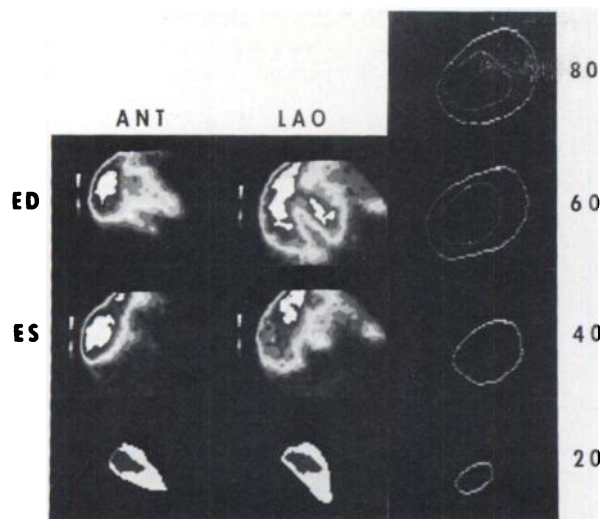


FIG. 7. Case study of idiopathic hypertrophic subaortic stenosis shown in format similar to that of Fig. 6. Note two lower reconstructions, where ES is not visualized.

preliminary nature of this investigation, as well as the addition of refinements discussed below, the patient studies are presented as examples demonstrating the implementation of the algorithm.

DISCUSSION

The algorithm described here is essentially an analytical solution to the reconstruction problem. Analytical solutions are also theoretically applicable to conventional ECT and TCT, but computer limitations necessitate the use of the more expedient backprojection or Fourier-based solutions. In contrast, the unique characteristics of the labeled LV blood pool permit the use of an analytical solution that requires only a single pair of coplanar views. By restricting the requisite views to those usually acquired in a conventional projective study, the tomographic reconstruction is automatically facilitated without any alteration of the clinical imaging procedure. This tomographic reconstruction complements the associated gated LV blood-pool study, since the objectives of both are the quantification and characterization of the ventricular wall during the cardiac cycle.

Several modifications to acquisition and processing are being examined. In particular, the use of a bilateral parallel-hole collimator (convergent in the range 45° – 60°) is ideally suited to this technique. When the two projections have been acquired separately using a conventionally collimated camera, the centroids of each contour are placed in coincidence to provide a reference for the relative lateral (x-dimension) positioning of the data. This alignment is critical to the accurate reconstruction of the tomograms in the scaling subroutine (Fig. 3D), which requires a superpositioning of the mirror-symmetric contour pair. The simultaneous acquisition of both projections using the bilateral collimator

not only eliminates the alignment problem but also cuts the imaging time in half.

Processing time associated with the reconstruction subroutines can be reduced by an order of magnitude. The only subjective operator-computer interaction is confined to the conventional gated processing, in which the anatomical region correlating to the LV is identified. The reconstruction subroutines themselves are essentially objective maximization computations dealing with only 25 to 40 pairs of data values. In contrast to conventional ECT, these computations require relatively little actual processing time on typical nuclear medicine computer systems to the extent that real-time tomography is feasible.

The digital aspect of the wall tomograms is ideally suited to the quantitative evaluation of parameters, including local wall velocities, absolute volumes, and transverse regional ejection fractions. The absolute LV volumes are derived from a scaling subroutine that relates detected counts to physical dimensions. These LV volumes, in turn, yield stroke volumes and cardiac outputs. This quantification, in conjunction with the tomograms and the conventional pair of gated views, provides a comprehensive assessment of LV function.

FOOTNOTES

- * Searle Pho Gamma IV.
- † MDS BICAM Computer.

REFERENCES

1. KUHL DE, EDWARDS RQ: Image separation radioisotope scanning. *Radiology* 80:653–662, 1963
2. KUHL DE, EDWARDS RQ: Reorganizing data from transverse section scans of the brain using digital processing. *Radiology* 91:975–983, 1968
3. CHESLER DA: Three-dimensional activity distribution from multiple positron scintigraphs. *J Nucl Med* 12:347–348, 1971
4. BUDINGER TF, GULLBERG GT: Three-dimensional reconstruction in nuclear medicine by iterative least-squares and Fourier transform techniques. *IEEE Trans Nucl Sci* NS-21:2–20, 1974
5. PHELPS ME, HOFFMAN EJ, MULLANI N, et al: Application of annihilation coincidence detection to transaxial reconstruction tomography. *J Nucl Med* 16:210–224, 1975
6. KEYES JW, KAY DB, SIMON W: Digital reconstruction of three-dimensional radionuclide images. *J Nucl Med* 14: 628–629, 1973
7. CORMACK AM: Representation of a function by its line integrals, with some radiological applications. *J Appl Phys* 34:2722–2727, 1963
8. CORMACK AM: Reconstruction of densities from their projections, with applications in radiological physics. *Phys Med Biol* 18: 195–207, 1973
9. HOUNSFIELD GN: Computerized transverse axial scanning (tomography): Part 1 Description of system. *Br J Radiol* 46:1016–1022, 1973
10. KEYES JW, ORLANDEA N, HEETDERKS WJ, et al: The humongotron—a scintillation camera transaxial tomograph.

- J Nucl Med* 8:381-387, 1977
11. JASZCZAK RJ, MURPHY PH, HUARD D, et al: Radionuclide emission computed tomography of the head with ^{99m}Tc and scintillation camera. *J Nucl Med* 18:373-380, 1977
 12. ROGERS WL, HAN KS, JONES LW, et al: Application of Fresnel zone plate to gamma-ray imaging. *J Nucl Med* 13: 612-615, 1972
 13. BARRETT HH: Fresnel zone plate imaging in nuclear medicine. *J Nucl Med* 13:382-385, 1972
 14. BUDINGER TF, MACDONALD B: Reconstruction of the Fresnel-coded gamma camera image by digital computer. *J Nucl Med* 16:309-313, 1975
 15. MUEHLLEHNER G: Rotating collimator tomography. *J Nucl Med* 11:347, 1970 (abst)
 16. VOGEL RA, KIRCH D, LEFEE M, et al: A new method of multiplanar emission tomography using a seven-pin-hole collimator and Anger scintillation camera. *J Nucl Med* 19: 648-654, 1978
 17. MIRELL SG, HECHT HS, BLAHD WH: Dynamic cardiac emission computed tomography from conventional gated equilibrium acquisitions. *Circulation* 60 (II):11-26, 1979 (abst)
 18. LEWIS M, BUJA LM, SAFFER S, et al: Experimental infarct sizing using computer processing and a three-dimensional model. *Science* 197:167-169, 1977
 19. ASAHARA A, UEDA H, WAKABAYASH S: A study of three-dimensional image expression of the left ventricle. *S Eur J Nucl Med* 5:221-228, 1980

THE SOCIETY OF NUCLEAR MEDICINE 29th Annual Meeting

June 15-18, 1982

Miami Beach Convention Center

Miami Beach, Florida

Call for Scientific Exhibits "One Picture Is Worth a Thousand Words"

The Scientific Exhibits Subcommittee welcomes the display of scientific exhibits at the 29th Annual Meeting in Miami Beach, Florida, June 15-18, 1982. A visual discipline like nuclear medicine is particularly suited for information exchange via an exhibit format which allows the viewer good time to study, criticize, and assimilate the material; exhibits can also supplement a presented paper and provide an alternative route for the author to get his message across. Exhibits may be large or small, free standing, displayed on a posterboard, or illuminated by a viewbox, but must conform to minimal standards.

Scientific awards, based on scientific merit, originality, appearance, and other criteria will be presented in several categories this year. Abstracts selected for presentation as scientific exhibits will be published in a separate brochure that will be distributed to all those who attend the meeting.

To present a scientific exhibit, please submit an abstract of your work on the official abstract form, which can be obtained by calling or writing:

Society of Nuclear Medicine
Att: Abstracts
475 Park Avenue South
New York, NY 10016
Tel: (212)889-0717

**Abstracts must be submitted on the official form and received (not postmarked)
by no later than Tuesday, February 23, 1982.**

SNM REFERRAL SERVICE

The SNM Referral Service is accepting applications from employers and job applicants. The Service lists positions wanted and positions available in the following nuclear medicine fields: Physician, Technologist, Scientist, Commercial, and Other.

The fee for job applicants is \$5.00 for SNM members and \$50.00 for nonmembers. For employers, the fee is \$50.00 for each position listed.

To obtain more information and an application form, please write to:

Referral Service
Society of Nuclear Medicine
475 Park Avenue South
New York, NY 10016